Noise Underlies Switching Behavior of the Bacterial Flagellum

Heungwon Park,[†] Panos Oikonomou,[‡] Calin C. Guet,[‡] and Philippe Cluzel[‡*]
[†]The James Franck Institute, University of Chicago, Chicago, Illinois; and [‡]FAS Center for Systems Biology and Department of Molecular and Cellular Biology, School of Engineering and Applied Sciences, Harvard University, Cambridge, Massachusetts

ABSTRACT We report the switching behavior of the full bacterial flagellum system that includes the filament and the motor in wild-type *Escherichia coli* cells. In sorting the motor behavior by the clockwise bias, we find that the distributions of the clockwise (CW) and counterclockwise (CCW) intervals are either exponential or nonexponential with long tails. At low bias, CW intervals are exponentially distributed and CCW intervals exhibit long tails. At intermediate CW bias (0.5) both CW and CCW intervals are mainly exponentially distributed. A simple model suggests that these two distinct switching behaviors are governed by the presence of signaling noise within the chemotaxis network. Low noise yields exponentially distributed intervals, whereas large noise yields nonexponential behavior with long tails. These drastically different motor statistics may play a role in optimizing bacterial behavior for a wide range of environmental conditions.

INTRODUCTION

Bacterial chemotaxis is a locomotion system that allows bacteria to move toward or away from sources of chemical attractants or repellants (1,2). In a liquid environment, *Escherichia coli* cells swim using rotary motors that power several long flagella. Over the last decades, a series of high-quality experiments have characterized the switching behavior of the flagellar motor in *E. coli*. So far, experiments have focused either on very short timescales in order to characterize the underlying molecular mechanism that induces the switch in the rotation of individual motors (3–5) or on very long timescales to characterize the slow temporal fluctuations of the switching rate of the motor (6,7). Recent work has shown that the coupling between the motor and the full flagellum filament can change the dynamics of switching on short timescales (4,8). Therefore, we present a systematic study of the behavior of the full flagellum apparatus that includes the filament and the motor for long and short timescales.

We characterize this behavior as a function of different cellular states. We also demonstrate how a simple phenomenological model that includes the noise of the signaling pathway can explain the observed behavior.

When motors rotate counterclockwise (CCW) the flagella form a stable bundle that acts as a propeller and bacterial swimming exhibits smooth runs. Clockwise (CW) rotation destabilizes the bundle and induces tumbles that randomize the trajectory of swimming bacteria (9). A signal transduction pathway translates temporal changes in the chemical environment into varying levels of activity of the histidine-kinase receptor complexes. The kinase, CheA, phosphorylates a response regulator, CheY, into its activated form CheY-P (10), which binds the basal part of the rotary motors (11–13) to induce tumbles (CW rotations) from the default CCW rotation. Single-cell studies have established a strict relationship between the output of the chemotaxis network, [CheY-P], and the probability for the motor to rotate in the clockwise directions, the CW bias (14).

In this work, we sort individual cells by their CW bias using 1500-s-long observations of switching behavior, similar to Korobkova et al. (4). Cells were attached onto a glass coverslip as in Park et al. (7). We recorded a 1500-s binary time series of motor switching events of CW and CCW rotations (data are from Park et al. (7)). We built histograms of CCW and CW interval lengths for each distinct cellular state defined by the CW bias. The allowed minimum time duration was 0.1 s (binning size). We normalized the histograms by the total number of events, whose normalized bins are called ρ_j, such that the sum of ρ_j is equal to 1. Thus, we normalized the histograms as $1 = \sum_{j=1}^{j_{\max}} \rho_j$ (for j^{th} bin) and calculated the associated cumulative distributions that are defined as $\rho_{C,j} = \sum_{k=j}^{k_{\max}} \rho_k$ (for j^{th} bin), where $k_{\max}$ is the last bin corresponding to the longest time duration. This associated cumulative distribution has a form of *1-C*, where *C* is the usual cumulative distribution. Due to the low number of events at long timescales, it is in general difficult to characterize the shape of the distribution with normalized distributions (ρ_j). By contrast, the cumulative distribution ($\rho_{C,j}$) exhibits a smoother profile at long timescale than the normalized distribution (ρ_j) because it is qualitatively the integrative form of the normalized distribution. Therefore, we used cumulative distributions to characterize the distribution patterns at short and long timescales.

Submitted June 22, 2011, and accepted for publication September 23, 2011.

*Correspondence: cluzel@mcb.harvard.edu

Heungwon Park's current address is Institute for Genome Sciences and Policy, Duke University, Durham, NC.

Panos Oikonomou's current address is Department of Molecular Biology, Princeton University, Princeton, NJ.

Calin C. Guet's current address is IST Austria, Am Campus 1, Klosterneuburg, Austria.

Editor: Charles W. Wolgemuth.

0006-3495/11/11/2336/5 $2.00

doi: 10.1016/j.bpj.2011.09.040

MATERIALS AND METHODS

Bacterial strains and plasmids

We used the wild-type *E. coli* strain RP437 (15). To obtain cells with high CW biases, we transformed RP437 cells with the plasmid pZE21-CheR that carries a TetR-inducible promoter that controls expression of *cheR* (7). To modulate the expression of the TetR-inducible *cheR*, we used the plasmid pZS4-Int1 that carries *tetR* under a constitutive promoter (7).

Simulations of temporal fluctuations in [CheY-P] from experimental measurements of the correlation time τ_{CheYp} and the variance $\sigma^2{}_{CheYp}$

We generated temporal fluctuations in [CheY-P] about a well-defined steady state ($\overline{Yp}$) using the Langevin equation:

$$\dot{\delta Yp} = -\frac{\delta Y_P}{\tau_{CheYp}} + \eta(t).$$

Here δYp represents the fluctuations in [CheY-P] around $\overline{Yp}$, τ_{CheYp} is the correlation time of the [CheY-P] fluctuations, and $\eta(t)$ is a Gaussian white noise term satisfying $\overline{\eta(t)} = 0$ and $\overline{\eta(t)\cdot\eta(t')} = \sigma_\eta^2 \cdot \delta(t-t')$. Using this Langevin equation, the fluctuating concentration of CheY-P can be expressed using the following exact Ornstein-Uhlenbeck formula (16):

$$\delta Yp(t+\Delta t) = \delta Yp(t)\cdot e^{-\left(1/\tau_{CheYp}\right)\Delta t} + \left[\sigma^2_{CheYp}\cdot\left(1-e^{-\left(2/\tau_{CheYp}\right)\Delta t}\right)\right]^{\frac{1}{2}}\cdot n_n,$$

Here n_n is the unit normal random variable between 0 and 1, and we used $\Delta t = 0.01$ s in our numerical simulations. The Monte Carlo simulation for this Ornstein-Uhlenbeck process (16) generates temporal fluctuations $\delta Yp(t)$ in [CheY-P] about $\overline{Yp}$ that corresponds to a specific CW bias. The functional relationship between the CW bias (b) and $\overline{Yp}$ is given as

$$b = \frac{\overline{Yp}^{N_H}}{\left(K_M^{N_H} + \overline{Yp}^{N_H}\right)},$$

where N_H (Hill coefficient) = 10.3 and $K_M = 3.1$ μM (14).

To generate $\delta Yp(t)$, we used the variance $\sigma^2{}_{CheYp}$ and the correlation time τ_{CheYp} of the fluctuating [CheY-P] measured from experimental time series (see Table S1 in the Supporting Material; such table was obtained from Park et al. (7)). We chose the Gaussian distributions $(f(Yp-\overline{Yp})_{\sigma_{CheYp}})$ to model the fluctuations in [CheY-P] (Yp) with mean $\overline{Yp}$ and the standard deviation σ_{CheYp} measured from experimental time series (7):

$$f(Yp-\overline{Yp})_{\sigma_{CheYp}} = \frac{1}{\sqrt{2\pi\sigma^2_{CheYp}}} e^{-\frac{(Yp-\overline{Yp})^2}{2\sigma^2_{CheYp}}}.$$

Table S1 shows $\sigma^2{}_{CheYp}$ for each CW bias bin. For each bin, we used the steady-state $\overline{Yp}$ corresponding to the CW bias (14).

Gamma-distribution

Two parameters, i.e., the Poisson rate ν and the number of hidden steps r in the γ-distributions $G_r(\nu,\tau)$, where τ is interval length, can be expressed as a function of the CW bias (b), which is also a function of Yp given as $b = Yp^{N_H}/(K_M^{N_H} + Yp^{N_H})$. Therefore we express the γ-distributions as a function of b, i.e., as a function of [CheY-P]:

$$G_r(\nu,\tau) = \frac{\nu^r\tau^{r-1}\exp(-\nu\tau)}{\Gamma(r)} = G_{r(b(Yp))}(\nu(b(Yp)),\tau) = G_{r(Yp)}(\nu(Yp),\tau),$$

where $\Gamma(r)$ is the γ-function. Here, the approximate functional forms of r and ν are given as $r_{CCW} = 8b+1$ for $0 \le b \le 0.5$, $r_{CCW} = 5$ for $0.5 \le b < 1.0$, $r_{CW} = 5$ for $0 \le b \le 0.5$, $r_{CW} = -8b+9$ for $0.5 \le b < 1.0$, $\nu_{CCW} = 2\omega_O \cdot b \cdot (8b+1)$ for $0 \le b \le 0.5$, $\nu_{CCW} = 2\omega_O \cdot b \cdot 5$ for $0.5 \le b < 1.0$, $\nu_{CW} = 2\omega_O \cdot (1-b) \cdot 5$ for $0 \le b \le 0.5$, and $\nu_{CW} = 2\omega_O \cdot (1-b) \cdot (-8b+9)$ for $0.5 \le b < 1.0$ (see Fig. S2 in the Supporting Material).

Convolution of the γ-distributions of the CCW and CW interval lengths

Using the functional relationships described above, we perform the convolution of the γ-distributions with the Gaussian noise distributions:

$$G_{r(\overline{Yp})}(\nu(\overline{Yp}),\tau)' = \int_{-\infty}^{\infty} f(Yp-\overline{Yp})\cdot G_{r(Yp)}(\nu(Yp),\tau)\cdot dYp.$$

To numerically calculate this convolution, we used $dYp = 0.01$ μM and the integration range is 0.01 μM $\le Yp \le$ 10.0 μM. The convoluted γ-distributions reflect the effects of noise in [CheY-P] on the switching behavior of the motor. The cumulative distribution is given by

$$G_{r(\overline{Yp})}(\nu(\overline{Yp}),\tau)'|_{Cumulative} = \int_{\tau}^{\tau_{\max}} G_{r(\overline{Yp})}(\nu(\overline{Yp}),\tau')'\cdot d\tau',$$

where we used $\tau_{\max} = 300$ s as an upper limit for the possible time duration.

Two-state free energy model (Tu-Grinstein model)

In the Tu-Grinstein model (17), CheY-P whose concentration is regulated by the upstream adaptive network interacts with bacterial motors to produce the switching events between CCW and CW rotational states. The CCW and CW rotational states are represented by two free energy wells that correspond to F_0 and F_1, respectively (see Fig. 2, later). The free energy barriers $\Delta F_0(Yp)$ and $\Delta F_1(Yp)$ govern the switching from CCW to CW and from CW to CCW, respectively. Temporal fluctuations in [CheY-P] (Yp) cause variations of the amplitude of these barriers. According to this model, the switching rates from CCW to CW (k_{01}) and from CW to CCW (k_{10}) are given as

$$k_{01} = 2\omega_0 \exp\left(\frac{-\Delta F_0(Yp)}{k_B T}\right) \text{ and } k_{10} = 2\omega_0 \exp\left(\frac{-\Delta F_1(Yp)}{k_B T}\right),$$

where ω_0, k_B, and T are the maximum total switching frequency (~1.9 s^{-1} from Korobkova et al. (4)), Boltzmann constant and absolute temperature, respectively. Here $Yp(t)$ is a temporally fluctuating function about the steady-state value ($\overline{Yp}$):

$$Yp(t) = \overline{Yp} + \delta Yp(t).$$

When $\delta Yp(t)$ is much smaller than the steady state value, the variations of the energy barriers can be approximately expressed by their linear expansion as in Tu and Grinstein (17),

$$\frac{\Delta F_{0,1}(Yp)}{k_BT} \cong \frac{\Delta F_{0,1}(\overline{Yp})}{k_BT} + \alpha_{0,1}\frac{\delta Yp}{\overline{Yp}},$$

where

$$\alpha_{0,1} \equiv \left.\frac{\partial \Delta F_{0,1}}{k_BT\partial \ln Yp}\right|_{Yp=\overline{Yp}}.$$

The switching of the motor can be described by using the following reaction equation:

$$\frac{db}{dt} = k_{01}(1-b) - k_{10}b,$$

where b is the CW bias. As shown in Cluzel et al. (14), the mutant cells with a disrupted network have a Hill-function-like relationship between the CW bias and the concentration of signaling molecules: $b = \overline{Yp}^{N_H}/(K_M^{N_H} + \overline{Yp}^{N_H})$.

In our previous study (4), we found the switching rates of the steady state of the motor are approximately given by Fig. S2 *A*:

$$k_{01}|_b \approx 2\omega_0 b = 2\omega_0 \frac{\overline{Yp}^{N_H}}{K_M^{N_H} + \overline{Yp}^{N_H}}$$

and

$$k_{10}|_b \approx 2\omega_0(1-b) = 2\omega_0 \frac{K_M^{N_H}}{K_M^{N_H} + \overline{Yp}^{N_H}},$$

where ω_0 is the maximum total switching frequency (~1.9 s^{-1} from Korobkova et al. (4)). Using these relationships and the two-state free energy model of the bacterial motor (see Fig. 2, later), the switching rates between CCW and CW states with small fluctuations (δYp) in [CheY-P] about the steady-state ($\overline{Yp}$) are given by

$$k_{01} = 2\omega_0 \cdot \frac{\overline{Yp}^{N_H}}{K_M^{N_H} + \overline{Yp}^{N_H}} \cdot \exp\left[-\alpha_0 \cdot \frac{\delta Yp}{\overline{Yp}}\right]$$

and

$$k_{10} = 2\omega_0 \cdot \frac{K_M^{N_H}}{K_M^{N_H} + \overline{Yp}^{N_H}} \cdot \exp\left[-\alpha_1 \cdot \frac{\delta Yp}{\overline{Yp}}\right].$$

In addition, we can find that free energy barriers $\Delta F_0(\overline{Yp})$ and $\Delta F_1(\overline{Yp})$ for a steady concentration ($\overline{Yp}$) of [CheY-P] are given by

$$\Delta F_0(\overline{Yp}) = k_BT \cdot \ln\left[\frac{K_M^{N_H} + \overline{Yp}^{N_H}}{\overline{Yp}^{N_H}}\right]$$

and

$$\Delta F_1(\overline{Yp}) = k_BT \cdot \ln\left[\frac{K_M^{N_H} + \overline{Yp}^{N_H}}{K_M^{N_H}}\right].$$

RESULTS

We observe that bacteria with low CW bias exhibit distributions of CCW intervals with power-law-like heavy tails that are not exponentially distributed (Fig. 1). By contrast, CW intervals are exponentially distributed. At higher CW bias of ~0.5, both CW and CCW interval distributions are similar and the nonexponential tails tend to disappear. Under our growth conditions, wild-type cells did not exhibit CW bias >0.6.

To explain the origin of the observed asymmetry between CCW and CW interval distributions (Fig. 1), we use a two-state model of the motor whose free energy depends on the concentration of the response regulator CheY-P as in Tu and Grinstein (17). In this model (Fig. 2), the probability for the motor to be in the CCW or CW state is governed by the free energy difference between each state. This difference is itself controlled by the concentration of the response regulator CheY-P. For example, in the absence of CheY-P, the motor only exhibits CCW rotation, which corresponds to a single F_0 free energy well. Increasing [CheY-P] decreases the depth (ΔF_0) of the CCW free energy well and increases the depth (ΔF_1) of the CW well. Accordingly, the probability of CW rotation increases and the probability of CCW rotation decreases.

For a given steady concentration ($\overline{Yp}$) of [CheY-P], the free energy depths are given by $\Delta F_0(\overline{Yp}) = k_BT \cdot \ln[(K_M^{N_H} + \overline{Yp}^{N_H})/\overline{Yp}^{N_H}]$ and $\Delta F_1(\overline{Yp}) = k_BT \cdot \ln[(K_M^{N_H} + \overline{Yp}^{N_H})/K_M^{N_H}]$, where K_M, N_H, k_B, and T are the dissociation constant (3.1 μM), the Hill coefficient (10.3), Boltzmann constant, and absolute temperature, respectively (see Materials and Methods). This model qualitatively reproduces the exponential distributions of CCW and CW interval lengths for a fixed concentration of CheY-P. In particular, the CW and CCW are asymmetrically distributed for low CW bias (i.e., low steady [CheY-P]) and become symmetrically distributed for CW bias = 0.5 ([CheY-P]~ 3.1 μM). For higher values of CW bias, the CCW and CW distributions become asymmetrically distributed.

In wild-type cells, however, [CheY-P] fluctuates as a function of time due to the intrinsic dynamics of the upstream signaling network (Fig. 3, *top*). We use the experimentally observed evaluation of the [CheY-P] noise from Park et al. (7). By contrast, Korobkova et al. (4) studied the dynamical behavior of the flagellar filament in the absence of the chemotaxis network and the presence of a stably expressed activated CheY mutant. Under this condition, the CW and CCW intervals could accurately be described by a γ-distribution. Gamma distribution is a good phenomenological model at short timescale when the motor is decoupled from the network as demonstrated in Korobkova et al. (4). There exist other adequate models such as the conformation spread model (5). However, this latter model alone does not reproduce the observed peaking frequency present at short timescale in the power spectrum of the binary time series associated with switching events of individual motors (4), which is most likely caused by the coupling between the filament and the motor (8). Moreover, in the complete bacteria that include the signaling network, we must also consider

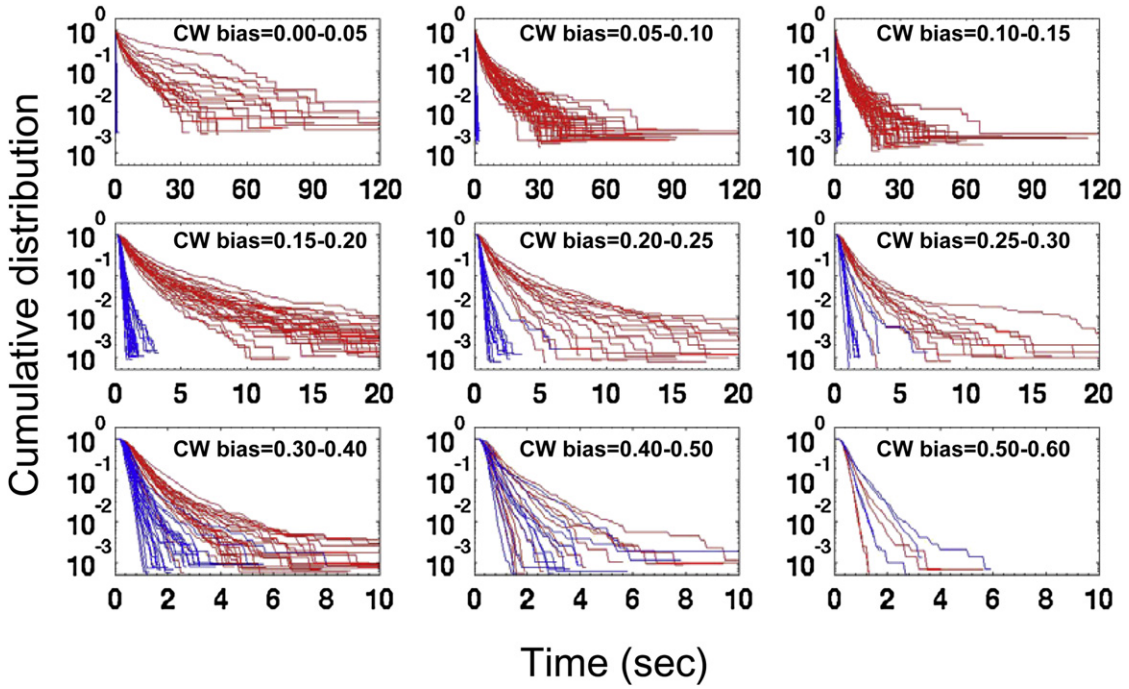

FIGURE 1 Cumulative distributions of CCW (*red*) and CW (*blue*) interval lengths from wild-type cells. Intervals are obtained from 1500-s binary time series in RP437 wild-type cells and RP437 cells expressing extra copies of CheR from pZE21-CheR plasmid (in Fig. S1, we marked RP437 wild-type cells as a point of reference by using different colors). We binned cells by their CW bias (note that the numbers in parentheses are the number of cells in each bin): 0.00–0.05 (18); 0.05–0.10 (44); 0.10–0.15 (41); 0.15–0.20 (33); 0.20–0.25 (17); 0.25–0.30 (13); 0.30–0.40 (26); 0.40–0.50 (12); and 0.50–0.60 (4).

the effect of long temporal fluctuations in [CheY-P]. In what to our knowledge is a new qualitative model, we combine the measured fluctuations of [CheY-P] from Park et al. (7) with the γ-distributed behavior of the flagellar filament to numerically calculate the CW and CCW interval distributions (Fig. 3, *bottom right*). This type of approach has been widely discussed in order to understand phenomena of rate processes with "dynamical disorder" in chemical physics (18,19).

For each CW bias, we performed the convolution of the noise in [CheY-P] (Fig. 3, *bottom left*) with the γ-distribution (Fig. 3, *bottom middle*) as obtained in Korobkova et al. (4). Our model explains the observed behavior for all ranges of CW bias. This calculation (see Fig. S2) illustrates that when the noise in [CheY-P] is absent, the distributions of CW and CCW intervals (Fig. 4 *A*) do not exhibit heavy tails at long timescales. By contrast, in the presence of correlated slow fluctuations of [CheY-P], the distribution of CCW intervals exhibits a heavy tail at long

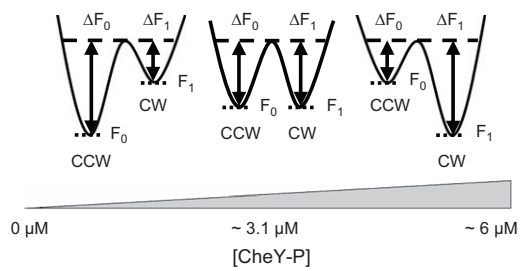

FIGURE 2 Free energy diagram of a simple two-state model of the bacterial motor. The values F_0 and F_1 are the free energies associated with CCW and CW rotation states, respectively (17). Increasing [CheY-P] (*blue gradient*) changes the free energy depths ΔF_0 and ΔF_1 (*arrows*).

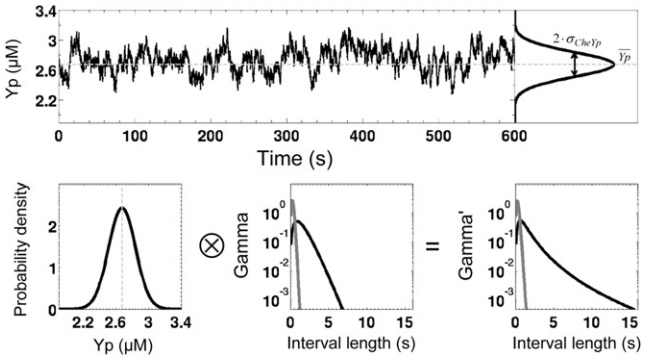

FIGURE 3 Effect of fluctuations in [CheY-P] on the switching behavior of the motor. (*Top panel*) Simulated temporal fluctuations $(Yp(t) = \overline{Yp} + \delta Yp(t))$ of [CheY-P] around the steady-state concentration $\overline{Yp}$ (*shaded dashed line*) corresponding to CW bias = 0.18, and with a variance $\sigma^2_{CheYp} = 0.027$ (μM^2) (7), typical for a cell with average wild-type behavior. We simulated temporal fluctuations in [CheY-P] using a Langevin equation given by $d\delta Yp/dt = -\delta Y_p/\tau_{CheYp} + \eta(t)$, where $\eta(t)$ is a Gaussian white noise term satisfying $\overline{\eta(t)} = 0$ and $\overline{\eta(t)\cdot\eta(t')} = \sigma^2_\eta \cdot \delta(t - t')$ (Material and Methods). This Gaussian distribution with variance σ^2_{CheYp} is used in the convolution process. (*Bottom panel*) Convolution ($\otimes$) of (*middle*) the γ-distributions (gamma) of CCW (*solid*) and CW (*shaded*) interval lengths obtained from cells with a steady level of [CheY-P] with (*left*) the Gaussian distribution of [CheY-P] with the standard deviation σ_{CheYp} (see Material and Methods). This convolution yields (*right*) stretched γ-distributions (gamma′) of the CCW (*solid*) and CW (*shaded*).

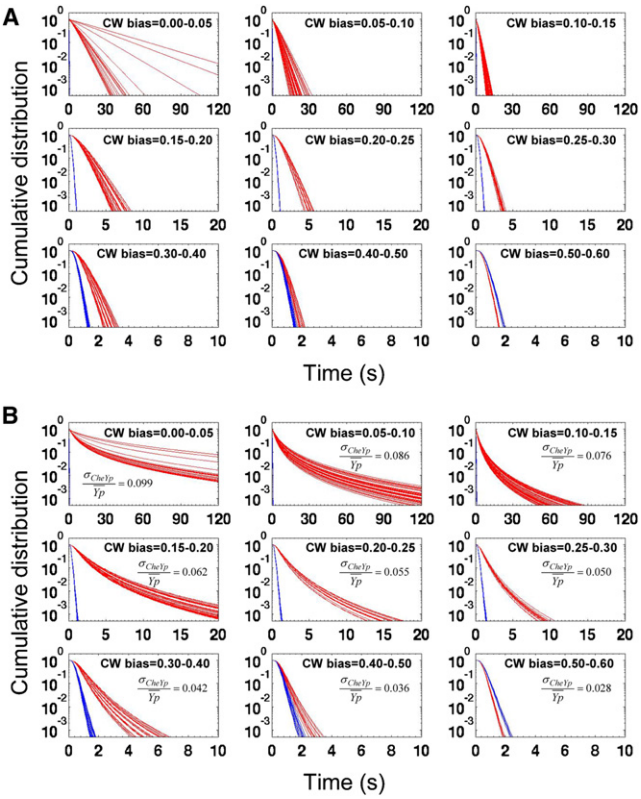

FIGURE 4 Numerical calculations using the scheme described in Fig. 3. (*A*) Cumulative γ-distributions of CCW and CW interval lengths without fluctuations in [CheY-P]. The steady states of [CheY-P] corresponded to the CW biases of the experimentally measured wild-type cells shown in Fig. 1. (*B*) Cumulative γ-distributions of CCW and CW interval lengths obtained from the convolution of Gaussian [CheY-P] noise distributions with γ-distributions from panel *A*. For each Gaussian distribution, we used σ_{CheYp} values (see Table S1) experimentally observed from Park et al. (7). (*Red*) CCW; (*blue*) CW. In each panel, $\sigma_{CheYp}/\overline{Yp}$ shows the relative noise of [CheY-P] to the steady state.

timescales, whereas CW intervals are exponentially distributed (Fig. 4 *B*). At higher CW bias with smaller [CheY-P] fluctuations, the numerical convolution (Fig. 4 *B*) shows that the distributions of both CW and CCW intervals tend to be exponentially distributed as in Fig. 4 *A*. Our results demonstrate how different phenotypic behaviors of bacterial locomotion emerge from the interactions between the signaling pathway fluctuations and the flagellar motor.

DISCUSSION

Knowing that distinct wild-type *E. coli* strains for chemotaxis display distinct switching motor behaviors, namely, some with exponentially distributed and some with nonexponentially distributed CCW intervals, it would be interesting to establish the relationship between chemotactic properties and the nature of distribution of the intervals. Because different switching statistics can be achieved by tuning the average level of [CheY-P] and its associated fluctuations, it is plausible that a specific environment can preferentially select bacterial strains with either an exponential or nonexponential switching behavior.

SUPPORTING MATERIAL

Two figures and one table are available at http://www.biophysj.org/biophysj/supplemental/S0006-3495(11)01131-3.

We thank Thierry Emonet and William Pontius for discussions. We thank Kathleen Dave for editing this manuscript.

This research was funded by National Science Foundation Division of Materials Research award 0213745 to the Materials Research Science and Engineering Centers at the University of Chicago, and National Institutes of Health award R01AI059195-03 to P.C.

REFERENCES

1. Adler, J. 1975. Chemotaxis in bacteria. *Annu. Rev. Biochem.* 44:341–356.
2. Adler, J. 1988. Chemotaxis—old and new. *Bot. Acta.* 101:93–100.
3. Block, S. M., J. E. Segall, and H. C. Berg. 1983. Adaptation kinetics in bacterial chemotaxis. *J. Bacteriol.* 154:312–323.
4. Korobkova, E. A., T. Emonet, …, P. Cluzel. 2006. Hidden stochastic nature of a single bacterial motor. *Phys. Rev. Lett.* 96:058105.
5. Bai, F., R. W. Branch, …, R. M. Berry. 2010. Conformational spread as a mechanism for cooperativity in the bacterial flagellar switch. *Science.* 327:685–689.
6. Korobkova, E., T. Emonet, …, P. Cluzel. 2004. From molecular noise to behavioral variability in a single bacterium. *Nature.* 428:574–578.
7. Park, H., W. Pontius, …, P. Cluzel. 2010. Interdependence of behavioral variability and response to small stimuli in bacteria. *Nature.* 468:819–823.
8. van Albada, S. B., S. Tănase-Nicola, and P. R. ten Wolde. 2009. The switching dynamics of the bacterial flagellar motor. *Mol. Syst. Biol.* 5:316.
9. Berg, H. C., and D. A. Brown. 1972. Chemotaxis in *Escherichia coli* analyzed by three-dimensional tracking. *Nature.* 239:500–504.
10. Stock, J. B., G. S. Lukat, and A. M. Stock. 1991. Bacterial chemotaxis and the molecular logic of intracellular signal transduction networks. *Annu. Rev. Biophys. Biophys. Chem.* 20:109–136.
11. Toker, A. S., and R. M. Macnab. 1997. Distinct regions of bacterial flagellar switch protein FliM interact with FliG, FliN and CheY. *J. Mol. Biol.* 273:623–634.
12. Welch, M., K. Oosawa, …, M. Eisenbach. 1993. Phosphorylation-dependent binding of a signal molecule to the flagellar switch of bacteria. *Proc. Natl. Acad. Sci. USA.* 90:8787–8791.
13. Welch, M., K. Oosawa, …, M. Eisenbach. 1994. Effects of phosphorylation, Mg^{2+}, and conformation of the chemotaxis protein CheY on its binding to the flagellar switch protein FliM. *Biochemistry.* 33:10470–10476.
14. Cluzel, P., M. Surette, and S. Leibler. 2000. An ultrasensitive bacterial motor revealed by monitoring signaling proteins in single cells. *Science.* 287:1652–1655.
15. Parkinson, J. S., and S. E. Houts. 1982. Isolation and behavior of *Escherichia coli* deletion mutants lacking chemotaxis functions. *J. Bacteriol.* 151:106–113.
16. Gillespie, D. T. 1996. The mathematics of Brownian motion and Johnson noise. *Am. J. Phys.* 64:225–240.
17. Tu, Y., and G. Grinstein. 2005. How white noise generates power-law switching in bacterial flagellar motors. *Phys. Rev. Lett.* 94:208101.
18. Zwanzig, R. 1990. Rate-processes with dynamic disorder. *Acc. Chem. Res.* 23:148–152.
19. Zwanzig, R. 1992. Dynamic disorder—passage through a fluctuating bottleneck. *J. Chem. Phys.* 97:3587–3589.